NMR Solution Structure of the 21 kDa Chaperone Protein DnaK Substrate Binding Domain: A Preview of Chaperone−Protein Interaction†

Hong Wang,‡,§ Alexander V. Kurochkin,‡ Yuxi Pang,‡ Weidong Hu,‡,|| Gregory C. Flynn,⊥ and Erik R. P. Zuiderweg*,‡

Biophysics Research Division, Department of Biological Chemistry, and Department of Chemistry, The University of Michigan, 930 North University Avenue, Ann Arbor, Michigan 48109, and Institute of Molecular Biology, University of Oregon, Eugene Oregon

Received January 12, 1998; Revised Manuscript Received March 25, 1998

ABSTRACT: The solution structure of the 21 kDa substrate-binding domain of the *Escherichia coli* Hsp70-chaperone protein DnaK (DnaK 386−561) has been determined to a precision of 1.00 Å (backbone of the β-domain) from 1075 experimental restraints obtained from multinuclear, multidimensional NMR experiments. The domain is observed to bind to its own C-terminus and offers a preview of the interaction of this chaperone with other proteins. The bound protein region is tightly held at a single amino acid position (a leucyl residue) that is buried in a deep pocket lined with conserved hydrophobic residues. A second hydrophobic binding site was identified using paramagnetically labeled peptides. It is located in a region close to the N-terminus of the domain and may constitute the allosteric region that links substrate-binding affinity with nucleotide binding in the Hsp70 chaperones.

DnaK is the Hsp70 (70 kDa heat shock protein) molecular chaperone protein of *Escherichia coli*. It was named (*1*) for its involvement in the replication process of bacteriophage λ in *E. coli*, but it plays a much more fundamental role in normal cellular growth and maintenance. Like all Hsp70 proteins, the expression of DnaK is greatly increased when *E. coli* is stressed by a variety of factors, including heat shock. Constitutively expressed, the molecular chaperone is involved in the in vivo folding and repair of proteins by binding to newly synthesized or partially unfolded polypeptides (*2*−*5*). Experiments using short peptides showed that DnaK, like other Hsp70s, preferentially binds to peptides rich in internal hydrophobic residues, and selects against negatively charged peptides. The smallest optimal binding size was found to be about seven amino acids long (*6*−*11*). DnaK has a slow ATPase activity (*12, 13*). Binding of ATP to DnaK stimulates the kinetics of (poly) peptide substrate binding and release (*14*), while the hydrolysis of ATP is accompanied by a slowing down of the substrate exchange kinetics.

DnaK interacts with the co-chaperones DnaJ and GrpE (*15*). DnaJ also binds to hydrophobic peptides while its binding to DnaK stimulates ATP hydrolysis by DnaK. GrpE has been shown to interact with the ATPase domain of DnaK and promotes nucleotide exchange by inducing conformational changes in the nucleotide binding site (*14, 16, 17*). A mixture of DnaK, ATP, DnaJ, and GrpE was able to refold luciferase in vivo, while the individual components were virtually ineffective in this assay (*18*). This demonstrated that the combined DnaK/DnaJ/GrpE system acts as a chaperone of protein folding just as the more well-known chaperonin system Gro-EL/Gro-ES (for a review, see ref *19*). As for the Gro-EL/Gro-ES system, ATPase activity is essential for the protein refolding potential of the DnaK/DnaJ/GrpE system (*18*), but what exact step in the reaction cycle requires this energy remains elusive as of yet (*14, 20*).

DnaK comprises three domains. The N-terminal 44 kDa fragment has the ATPase function and is therefore referred to as the ATPase domain (*21, 22*). The substrate-binding function of DnaK is solely associated with the C-terminal 27 kDa fragment (*23*). It was discovered that the 18 kDa domain immediately following the 44 kDa ATP-binding domain of the homologous Hsc70 chaperone has a peptide-binding affinity (8 μM) indistinguishable from that of the native Hsc70 (5−8 μM) for the S-peptide of RNase-A (*24*). It thus appears that all the substrate-binding determinants are located in an 18 kDa domain directly following the ATP-binding fragment, called peptide-binding domain (PBD). The full 27 kDa C-terminal fragment is not necessary for this function. The last 10 kDa domain may be involved in interaction with the co-chaperone DnaJ (*24*) and with the regulation of the substrate-binding affinity (*11, 23, 25*−*27*).

Members of the Hsp70 chaperone families are highly conserved among all species. Amino acid homology varies from 40% upward, with better conservation in the ATPase domain, slightly worse conservation in the substrate binding domain, and the least conservation in the C terminal domain (Figure 1). The three-dimensional structure of the 44 kDa ATPase domain of Hsc70 has been determined by X-ray

† This work was supported by the National Institutes of Health, Grant GM52421.

* To whom correspondence should be addressed. Biophysics Research Division and Departments of Biological Chemistry and Chemistry. E-mail: zuiderwe@umich.edu.

‡ Biophysics Research Division.

§ Present address: Abbott Laboratories, Abbott Park, Illinois 60064.

|| Present address: Memorial Sloan-Kettering Cancer Center, New York, NY 10021.

⊥ University of Oregon.

S0006-2960(98)00085-3 CCC: $15.00
Published on Web 05/14/1998

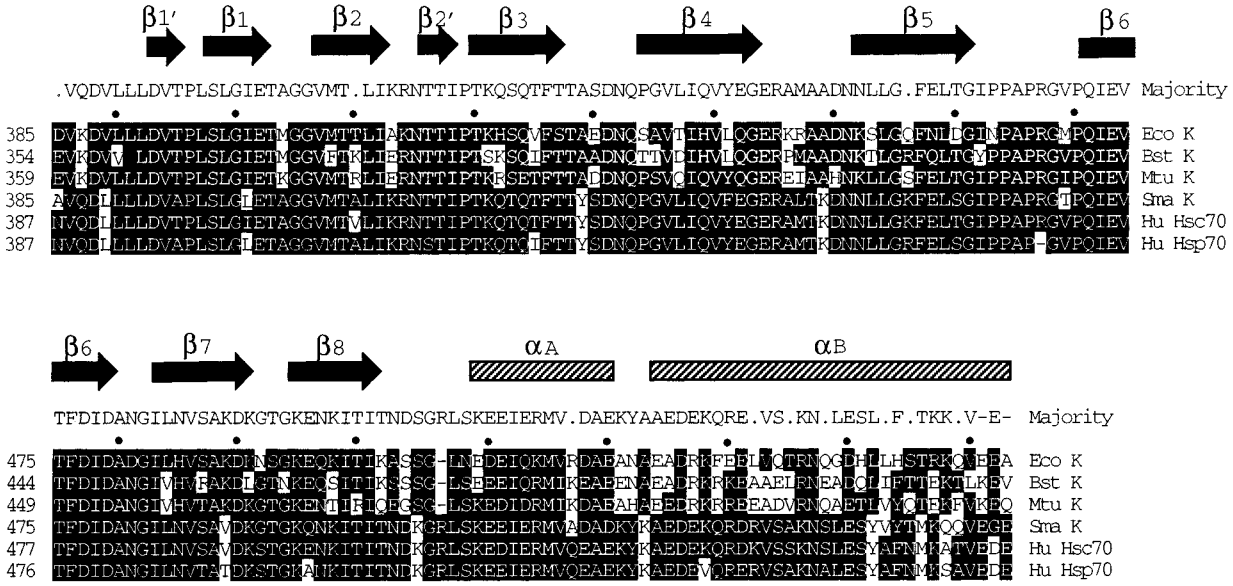

FIGURE 1: Alignment of the substrate-binding domains of six Hsp 70 proteins of different organisms. Numbering here and in this paper are as in ref *23*. The aligned protein sequences are the following: Eco K., *E. coli* DnaK (the protein studied in this paper); BstK, *stearothermopilus* DnaK; MtuK, M. *tuberculosis* DnaK; Sm Hsp70, *S. mansoni* Hsp70; Hu Hsc70, *Homo Sapiens* Hsc70; and Hu Hsp70, *Homo sapiens* Hsp70.

crystallography to a resolution of 2.2 Å (*21*). It is a two-lobed protein with a deep cleft in which ATP binds, very similar to the ATP-binding domains of G-actin and hexokinase. Recently, the crystal structure of the DnaK-ATPase domain bound to GrpE has been determined (*17*). Differences in conformation between the ATPase domain of this complex and that of the Hsc-ATPase domain (*21*) were taken to suggest that the geometry of the ATP-binding site changes upon GrpE binding, thus explaining the modulation of DnaK nucleotide binding by this factor.

The structure determinations of the substrate-binding domains of the Hsp70 chaperone proteins have been slow forthcoming, possibly due to the intrinsic aggregative behavior of such fragments. The first experimental structural information on this domain came from NMR spectroscopy (*28*). The study revealed that the secondary structure of the middle substrate-binding domain of Hsc70 has a β-strand topology not seen before in other proteins. An identical topology was found, also by NMR, for the substrate-binding domain of DnaK (*29*). The experimental topology of the molecule was found to be radically different from that suggested by homology modeling and secondary structure prediction (*30*).

Recently, a crystal structure of a 26 kDa substrate-binding domain of DnaK (the substrate-binding domain plus the majority of the 10 kDa C terminal domain, residues 389−603) with a bound peptide has been determined by X-ray diffraction at a resolution of 2.0 Å (*23*). The structure was found to consist of a β-sheet domain (with the topology as previously found (*28, 29*)), followed by an α-helical domain. A long transitional helix connects the two domains. The helix can be viewed as belonging to either one or both domains. It is very likely to be involved in the regulation of the substrate-binding function.

Here, we report the solution structure of a 21 kDa fragment of DnaK containing the β-sheet domain and the transitional helix of the substrate-binding domain (residues 381−561; numbering as in ref *23*). The structure was determined for residues 381−553 from multinuclear three- and four-dimensional NMR experiments and is one of the largest protein monomer structures solved by NMR to date. The structure highlights the active role of DnaK in protein (un)-folding and offers a preview of the interaction of this chaperone with other proteins. We also identified a second hydrophobic site that may be involved in the coupling mechanism of the ATPase and substrate-binding domains.

MATERIALS AND METHODS

Sample Preparation

Plasmid pDnaK386−561 was constructed by PCR amplification using p*KJ* (*31*) as a template. Primers were designed to introduce *Bam*H1 and *Hin*dIII restriction sites at the 5′ and 3′ ends of the amplified product, respectively. The PCR fragments were digested with the appropriate restriction endonucleases and ligated into the plasmid pQE30 (Qiagen). The resulting plasmid codes for amino acids 386−561 of DnaK (DnaK-substrate-binding domain or DnaK-SBD) fused to the N-terminal sequence MRGHHHHHHGSIEGR and was used to transform *E. coli* strain XL1-Blue. The non-native residues SIEGR could be observed in the NMR spectra and are referred to as residues 381−385. Up to 60 mg/L of fully $^{13}C/^{15}N$-labeled pure protein was obtained from cell cultures grown on a defined medium (*32*) containing 1 g/L ^{15}N-labeled ammonium chloride and 4 g/L [^{13}C]d_6-glucose (Isotech). The 190 amino acid protein (21 kDa) was affinity purified using a Ni-NTA resin column (Qiagen) according to manufacturer's recommendations. The N-terminal fusion peptide was not removed. This peptide was found to not interfere with the NMR experiments needed for structure determination.

NMR Spectroscopy

All NMR spectra were acquired on Bruker AMX500 and AMX600 spectrometers equipped with B_0-field gradient

triple-resonance probes. The experiments were carried out with 1−1.5 mM samples of ^{13}C and ^{15}N uniformly labeled DnaK-SBD, in 50 mM phosphate buffer, pH 7.0, 25 °C, using 5 mm probes except when stated otherwise. The spectra were processed with Felix software (a gift from Hare, Inc.) augmented with in-house written baseline line correction routines.

Assignments. Sequential backbone assignments for this 21 kDa protein domain, with a rotational correlation time of 13 ns, had to be based on the four most sensitive heteronuclear triple resonance experiments that transfer magnetization through one-bond scalar coupling. They are 3D constant-time HNCA (*33*), HN(CA)HA (*34, 35*), HN(CO)CA (*33*), and HA(CACO)NH (*36*). The pulse sequence of the HNCA experiment was modified to allow higher resolution along the constant time ^{15}N dimension without sacrificing sensitivity (*29*). Cross-polarization-driven (*37*−*40*) 3D H(C)CH-TOCSY (*41*), 3D (H)CCH-TOCSY (*42*), and 3D (H)C(CCACO)NH-TOCSY (*43*) were used to identify residue types for the assignment procedure and to obtain side-chain resonances. Side-chain assignments were further verified with a 3D carbon−carbon NOE spectrum (*44*). Data analysis was carried out by using a suite of in-house written UNIX AWK programs, a quick contour-viewing program called RGO (a gift from Glaxo-Wellcome Inc.), and an in-house written interface to the Felix program called Felixtalk. The backbone and side-chain assignments are 95% complete for residues 381−553. Resonances from the N-terminal histidine tag and from eight residues at the C-terminus were not observed in the ^{1}H-^{15}N HSQC and any of the triple resonance experiments and could therefore not be assigned.

NOE Experiments. To obtain distance restraints for the structure calculations, five heteronuclear-resolved NOESY spectra were acquired using 100 ms NOE mixing times on a Bruker AMX600 spectrometer. A ^{15}N-resolved 3D NOESY-HSQC spectrum (*45*) was collected with gradient water suppression using Watergate (*46*) with an uniformly ^{15}N-labeled sample in 90% H_2O/10% D_2O. To help resolve the extensive ambiguity in NOE peak identification, another ^{15}N-resolved 3D HMQC-NOESY-HSQC spectrum that labeled side-chain ^{13}C chemical shifts in one of the indirection dimensions was acquired using $^{15}N/^{13}C$ uniformly labeled protein. Two complimentary 3D ^{13}C resolved NOESY-HMQC spectra were recorded with the double-labeled sample dissolved in 100% D_2O, one with two ^{1}H dimensions and one ^{13}C dimension and another with one ^{1}H dimension and two ^{13}C dimensions. To unambiguously identify NOEs for initial structure calculation, a 4D ^{13}C-resolved HMQC−NOESY−HSQC spectrum (*47, 48*) was collected with a two-step phase cycling and extensive spectral folding around methyl groups to improve resolution. The 4D spectrum was acquired in 10 days using an 8 mm Nalorac gradient probe with a ^{15}N and ^{13}C uniformly labeled sample in D_2O solution.

Other NMR Experiments. Scalar Couplings. Three-bond scalar couplings defining the ϕ-dihedral angle were obtained from a 3D HNHA spectrum (*49*). Limits in signal/noise ratio (4 days data acquisition) allowed us to quantify only 75 scalar couplings. From those, only couplings smaller than 4 Hz or larger than 7 Hz were used to define dihedral ϕ restraints.

Dynamics. The backbone dynamics were obtained from the ^{15}N-relaxation experiments T_1, T_2, and ^{1}H-^{15}N NOE (*50, 51*). The data were used to obtain an estimate of the rotational correlation time of the protein (13 ns at 25 °C) and to qualitatively asses the flexibility of the peptide backbone as documented by the ^{1}H-^{15}N NOE data. Order parameter calculations have not been pursued in detail because the shape of protein molecule was found to be not spherical (28 × 36 × 45 Å) while the structure determination is currently of insufficient quality to define the directions of the N−H vectors with respect to the principal axes of the diffusion tensor with adequate precision (*52, 53*).

Peptide Binding. Variants of peptides K (KLIGVLSSLFRPK)[7], KLIGVLSSCFRPK, and KLIGVLCSLFRPK, kindly provided to us by Dr. G. Walker (MIT), and a peptide G (VKKRCSMWIIPTDDEA) as discovered by one of us (G.C.F.) were chemically modified with the paramagnetic label TEMPO at the cysteine sites. These paramagnetically labeled peptides were titrated into a 0.2 mM solution of ^{15}N-labeled DnaK-SBD while the ^{15}N-^{1}H amide shift correlation map was monitored by NMR. At the end of the titration experiment, the spin label was reduced with ascorbic acid in the NMR tube containing the mixture, and the ^{15}N-^{1}H amide shift correlation map was recorded as a control.

Structure Calculations

An ensemble of five initial structures based on the unambiguous 4D-derived NOEs was used to help resolve remaining ambiguities in NOE peak assignments from the complementary spectra described above. The resulting total number of NOE identifications is 1016 (region 386−553). Strong, medium, and weak NOE peaks were converted to NOE distance restraints with upper limits of 2.8, 3.5, and 5 Å, respectively. No lower limits were used. Standard pseudo-atom upper distance corrections were added (*54*), except for those methylene groups and valyl and leucyl double methyl groups if both of the stereoisotopomers displayed NOE to a particular proton. The distribution of the NOE restraints over the molecule is given in Figure 2. It is apparent that more long-range constraints are found for the β-domain (region 393−501) than for the α-helical section. In addition to the NOE distance restraints, generic distance restraints were used for the 58 hydrogen bonds in the regular secondary elements. Each hydrogen bond was represented by two distance restraints (N to O and HN to O) to preserve linear bond geometry. For every residue except for those preceding a proline residue, two dihedral restraints per peptide plane (O−C′−N−H and Cα-C′−N′−Cα) were used to enforce planarity. Upper and lower limits for the 59 ϕ restraints were estimated from the experimental scalar couplings by using the calibration curve as obtained by Bax and co-workers (*49*).

The structures were calculated using the InsightII program (Molecular Simulations, Inc.) on a Silicon Graphics, Inc. Challenge computer. A combined distance geometry/simulated annealing protocol was used to calculate the ensemble of structures. First, metric distance geometry program DGII was used to calculate an ensemble of 20 starting structures. For the distance geometry calculation, the upper and lower distance bound were first improved using a triangular smoothing method. Then the coordinates were embedded after a prospective metrization procedure to obtain the widest possible sampling of conformation space. Following a majorization step using constant weights Guttman

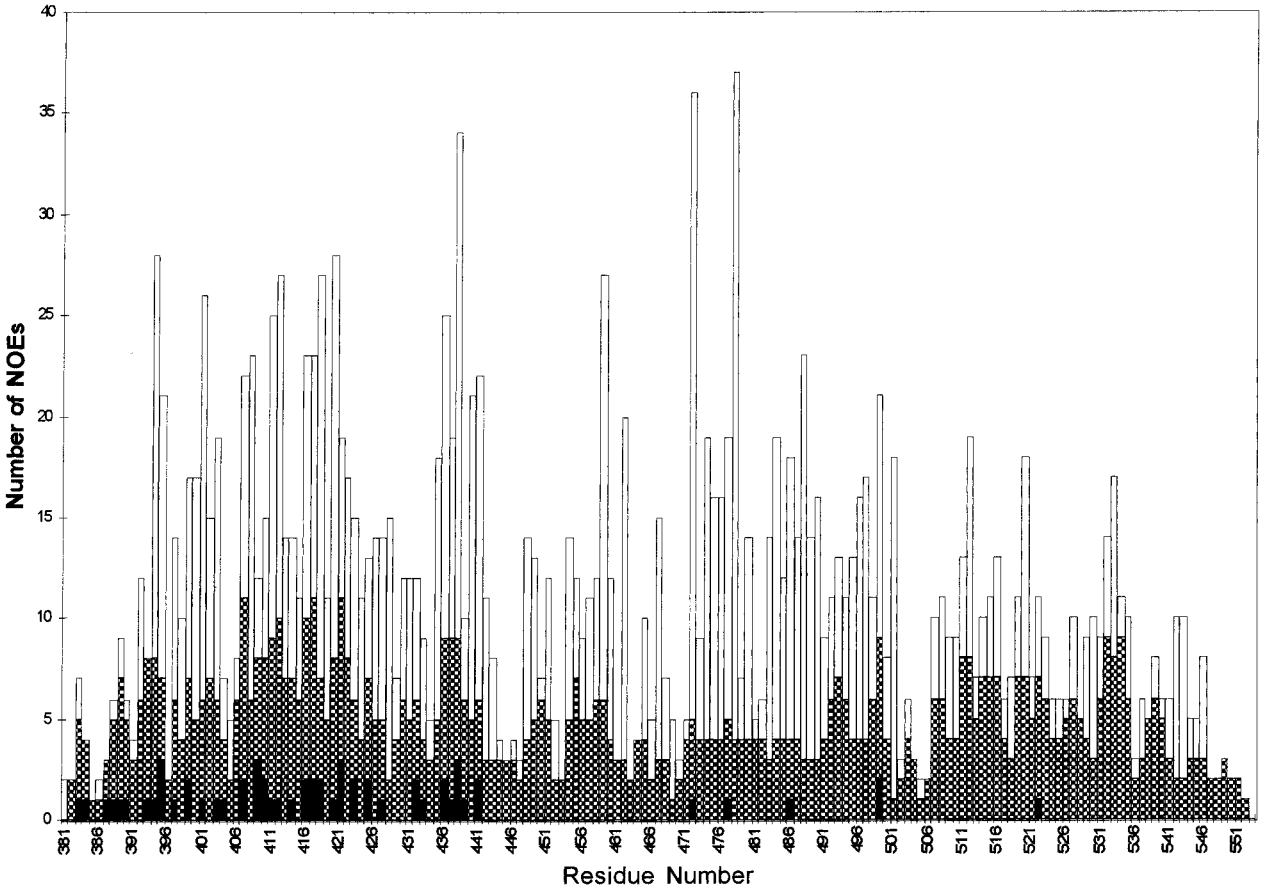

FIGURE 2: Distribution of NOE restraints in the DnaK 386−553. Indicated are intraresidue NOEs (black), sequential NOEs (crosshatched), and medium and longrange NOEs (white).

transformations, the coordinates were further optimized to reduce the constraint violations using a simple simulated annealing protocol of DGII (NMRchitect User Guide, 1993, Biosym Technologies). Each distance geometry structure was subsequently refined with five independent restrained molecular dynamics and simulated annealing runs, using a protocol similar to that described by Nilges et al. (*55*). Briefly, the starting structures were first minimized with normal covalent bond interactions and experimental restraints, but with very low noncovalent interactions to reduce any local hot spot. Then the kinetic energy was raised to 1000K and the conformational space was searched using molecular dynamics calculation for 4 ps. The protein was then slowly annealed to 300K in a 24 ps trajectory while increasing the nonbond interactions gradually to normal values. A quartic form nonbond interaction term with the atom radius scaled by 0.825 was used throughout the molecular dynamics/simulated annealing simulation to facilitate broader conformation space search. Finally, the structures were minimized using normal Leonard-Jones nonbonding interaction terms and experimental restraints. The CVFF force field as implemented in the DISCOVER version 2.9.5 was used in the calculation (Discover 2.9.5 User Guide, 1994, Biosym Technologies). A soft square function with a flat well was used as the potential for the distance and torsion angle constraints. Force constants were maintained at 377 kJ/mol/Å^2 for the NOE-derived distance restraints with a maximum force of 6285 kJ/mol/Å and at 314 kJ/mol/rad^2 for ϕ dihedral angle constraints with a maximum force of 1257 kcal/mol/rad. The statistics reported here are for the 25 structures with lowest total energy. These structures had good covalent geometry and few restraint violations (see Table 1). Average coordinates were computed for these 25 structures, and an extensive restrained energy minimization was carried out. Statistical data on the precision of the structure are given in Table 2. The coordinates of the average structure and of the ensemble of 25 best structures are available as Supporting Information.

RESULTS AND DISCUSSION

Overall Structure. The NMR structure of DnaK-SBD is based on 1016 NOE distance constraints and 59 experimental dihedral angle restraints and should be viewed as a medium-resolution result (β-domain 1.00 ± 0.19 Å backbone atoms; 1.56 ± 0.25 Å heavy atoms, see Tables 1 and 2 for computational details). An ensemble of the 25 lowest-energy structures is shown in Figure 3. No NMR data were obtained for the last eight residues, and all figures show the structure for the residues 386−553 only. Averaging and minimization of the 25 best structures lead to the structure shown as a cartoon in Figure 4. The molecule consists of a globular β-domain (residues 390−500) followed by a long kinked α-helix. An intriguing phenomenon is observed for the C-terminus of this helix: it is anchored into a groove in the β-domain. We have measured a rotational correlation time of 13 ns for this nominally 21 kDa domain, at 25 °C, from ^{15}N relaxation measurements (*50*). We observe very similar correlation times for T4-lysozyme (*56*) (19 kDa) and *E. coli* flavodoxin (*57*) (20 kDa), both monomeric molecules. DnaK-SBD is thus a monomer, and the observed self-binding

Table 1: Structure Calculation[a]

restraints		quality	
NOE		bond lengths	standard deviation = 0.01 Å
intra-residue $\{i,j\|j = i\}$	60		
sequential $\{i,j\|j = i + l\}$	384	bond angles	standard deviation = 2.5°
medium range $\{i,j\|j < i + 4\}$	138	peptide planes (ω)	standard deviation = 5.7°
long range $\{i,j\|j > i + 5\}$	434	dihedrals (ψ, ϕ)	91.5% in most favorable + additionally allowed regions (PROCHECK)
total	1016	internal energy	(Discover) 1281 kJ M^{-1}; 828 ± 31 kJ M^{-1}
		NOE energy	(Discover) 85 kJ M^{-1}; 52 ± 5.8 kJ M^{-1}
other distances		residual NOE	violations ≥ 0.1 Å
H-bonds			10 (out of 1016)
(2 per bond)	114		average of these = 0.16 Å
			largest violation = 0.34 Å
dihedrals			
ϕ	59		

[a] Quality parameters are given for the averaged and minimized structure. Energies are given for both the average minimized structure and the ensemble of 25 best structures.

Table 2: Structure Precision[a]

region of DnaK	RMSD backbone atoms	RMSD heavy atoms
all (386-553)	2.16 ± 0.26	2.80 ± 0.21
all (393−545)	1.42 ± 0.13	2.14 ± 0.15
β-domain (393−501)	1.00 ± 0.19	1.56 ± 0.25

[a] RMSD of the 25 accepted lowest energy structures to their average structure, given in angstroms. The average structure was calculated from a superposition of the backbone atoms (N−Cα-C′−O) of the β-domain and was not minimized for this calculation.

is intramolecular and not intermolecular. The overall dimensions of the molecule are 28 × 36 × 45 Å.

The β-domain is composed of residues 393−501 and is arranged in two large antiparallel β-sheets. The topology of the strands in these sheets has not been observed in any other class of proteins, but shows some resemblance to the immunoglobulin fold. The bottom sheet of the β-domain is made up of the four antiparallel strands 3, 6, 7, and 8 (see Figure 1 for nomenclature). This sheet is fairly regular and has the right-handed twist commonly observed in β-sheets. The top sheet consisting of strands 1, 2, 4, and 5 is highly irregular. The sub-sheet formed by strand 1 and strand 2 and the sub-sheet formed by strand 4 and 5 are both highly twisted with their inner loops bending upward. The two subsheets are almost orthogonal to each other.

The binding groove is between loops L1,2 (residues 403−406) and L3,4 (residues 428−434) and it is reinforced by the loops L4,5 (residues 444−450) and L5,6 (residues 462−470) through multiple van der Waals interactions (see Figure 4). The residues in L5,6 and L1,2 are mostly apolar while residues in L3,4 and L4,5 are mostly polar and/or charged. All loops have a well-defined structure, except for L5,6 (residues 462−470) which clearly shows diminished $^1H \rightarrow {}^{15}N$ NOEs (*50*) and hence is more dynamic (Figure 5).

The long α-helix runs from residue 507 to 532 and has a large kink between residues 518 and 523. Because of the large kink, the long helix wraps around the two loops L1,2 and L4,5 and makes multiple contacts with these two loops. It is interesting to note that we have been able to proteolytically cleave BiP (the Hsp70 from the endoplasmic reticulum) specifically at residues 509, 517, and 519 from a larger fragment (400−638) (GCF and ERPZ, unpublished). These locations correspond very precisely to the start and break in the helix in DnaK. We therefore predict that a helix also exists at this position in BiP and that it has kinks similar to those observed for DnaK.

Comparison with the Crystal Structure. Comparison of the solution structure of DnaK 386−553 with the crystal structure (*23*) reveals some interesting features about the structure and its substrate binding functionality. The crystal structure was determined for a larger construct of DnaK consisting of residues 389−607. A seven residue peptide (NRLLLTG) was bound to the protein. We superimposed the crystal structure with the minimized average NMR structure in Figure 6. The structure of the β-domain is virtually the same in both structures (RMS difference in backbone positions 2.20 Å). The major differences between the NMR structure and the crystal structure lie at the α-helical domain. Being a longer construct, the C-terminal α-helical domain in the crystal structure has several segments of helix forming a bundle. This helical domain covers the substrate binding groove. The construct we studied here by NMR is truncated and ordered up to residue 553, which is just short of the end (556) of the first long kinked α-helix in the crystal structure. The otherwise long helix is unwound in its middle section, and the unwound residues form a large loop and bind to the substrate binding groove in the β-domain in an extended conformation. The location where the α helix starts to unwind is at residue 535. The unwound area is dynamic in solution, whereas the bound tail area (540−547) has a more stable conformation, as gleaned from the $^1H \rightarrow {}^{15}N$ NOEs (*50*) in Figure 5. It was suggested from the comparison of the two crystal forms that the movement around the region 536−538 may be the conformation change needed for the opening of the binding groove. The current data suggests that much larger structural changes are possible (see also below). Another major difference between the NMR and X-ray data is the position of the αB helix relative to the β-domain. Figure 7 shows that in the crystal structure the helix runs on top of the loops L4,5, L1,2, and L3,4, while in the NMR structure this helix is swung much more to the backside of the loops and leaves the loops L4,5 and L1,2 more exposed to the solvent. This conformation is consistent with the fact that L4,5 is very hydrophilic.

The most striking feature from the comparison of the two structures is the conformation of the bound substrate. In the crystal structure, the substrate-binding site is occupied by a linear seven residue peptide; in the NMR structure, the very same site is occupied by the unwound C-terminus of the αB helix, also in an extended conformation (Figures 6 and 8). Residues ^{540}DHLLHSTR^{547} are involved in this

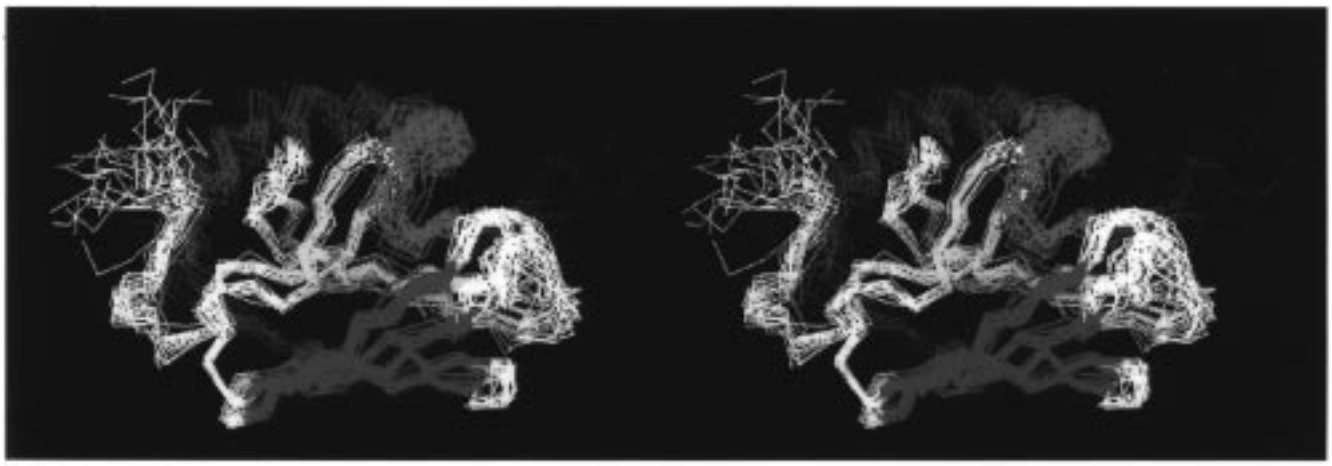

FIGURE 3: Ensemble of the 25 lowest-energy structures of the DnaK substrate-binding domain, residues 381−561, showing residues 386−553 only. The structures were determined from 3D and 4D heteronuclear NMR data and calculated from 1075 experimental constraints using a hybrid distance-geometry/simulated annealing protocol. The Cα-traces are shown. The RMSD over the β-domain is 0.96 ± 0.22 Å for the traces, 1.00 ± 0.19 Å for the backbone atoms and 1.56 ± 0.25 Å for all atoms. The color coding is as follows: light blue, the four stranded β-sheet comprising strands 3, 6, 7, and 8; yellow, the four stranded β-sheet comprising strands 1, 2, 4, and 5; red, the α-helical area and the "substrate"; white, other (for nomenclature see Figure 1).

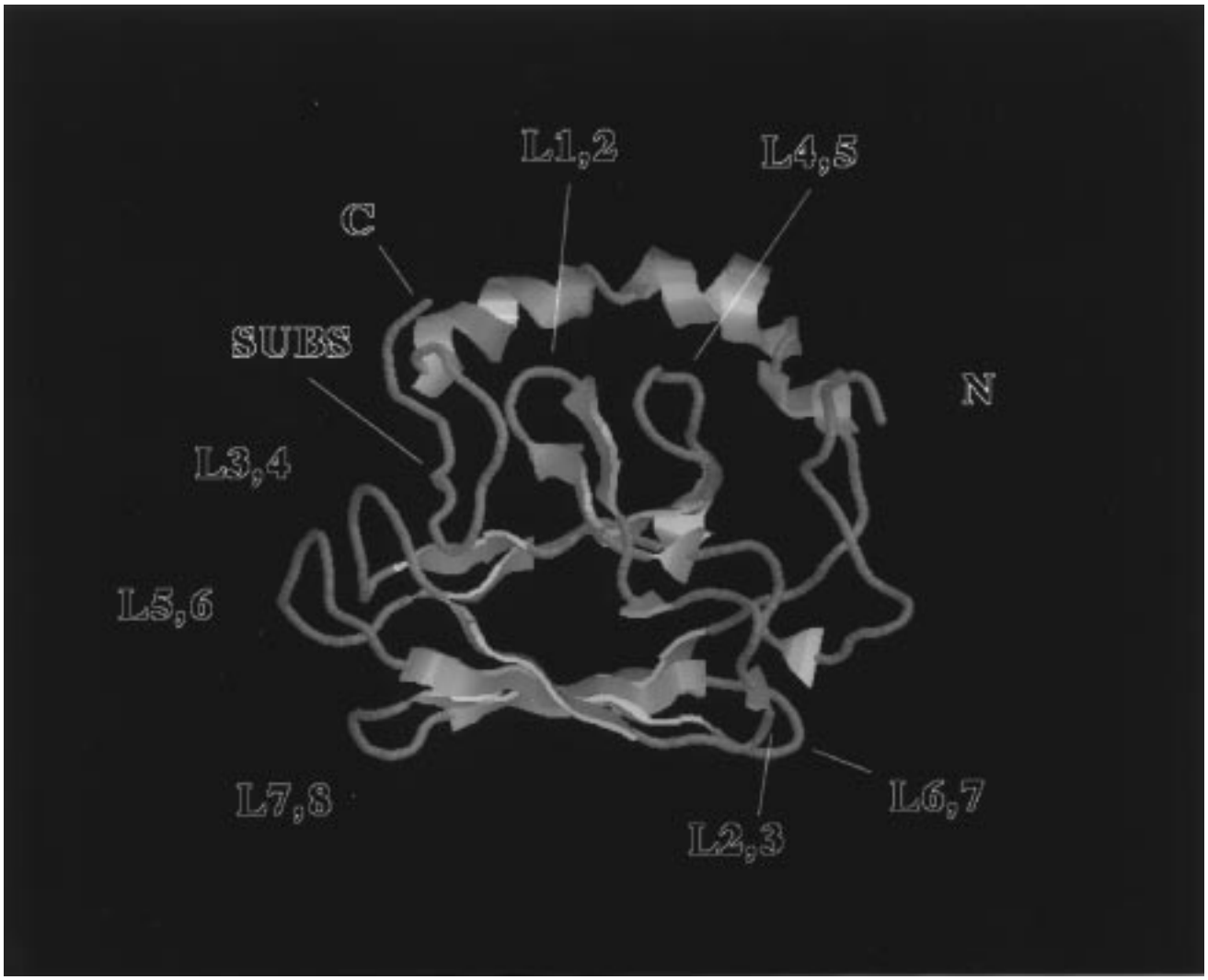

FIGURE 4: Cartoon of the minimized average of the ensemble of 25 NMR structures. β-strands are identified by arrows; the helix by a coil. The loop areas (e.g., L1,2), N- and C-terminus, and substrate are identified. The picture was generated with RasMac 2.6.

interaction. That the protein construct used for the NMR study binds to its own C-terminal tail may not be a surprise after all, considering the function of DnaK as a molecular chaperone and its function to bind to partially unfolded polypeptides. Here, one observes the interaction of DnaK with a protein (which happens to be itself) rather than with

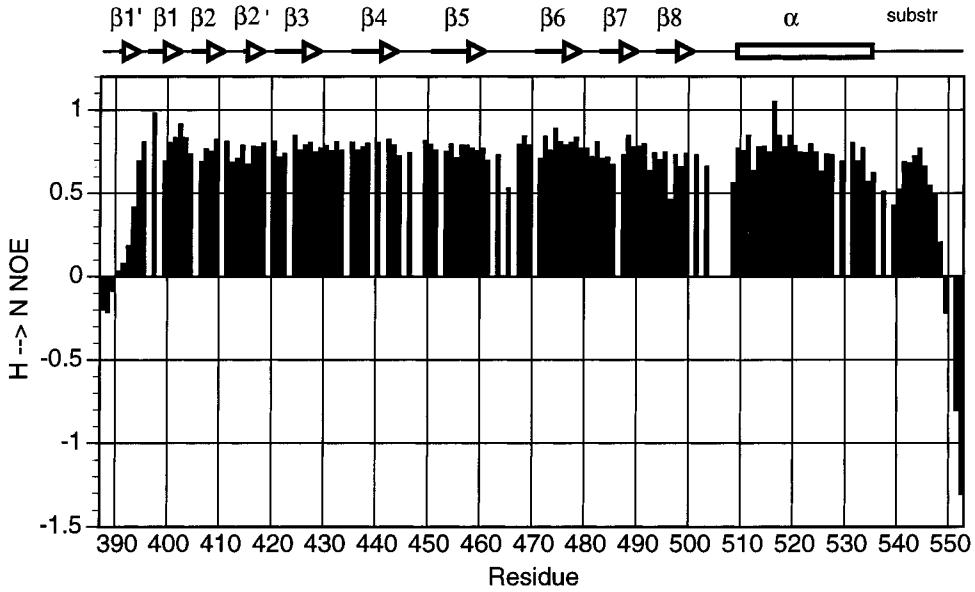

FIGURE 5: ^{1}H-^{15}N NOE data for DnaK−SBD 386−553. The data are the ratios of the intensities of ^{15}N-^{1}H NMR cross-peaks in inverse correlation spectra obtained with and without proton saturation using standard pulse sequences (*50*, *51*). NOEs smaller than 0.7 indicate residues that experience substantial local dynamics; NOEs larger than 0.7 indicate motionally restricted residues. Secondary structure elements (nomenclature in Figure 1) are indicated. "Substr" represents the pseudo-substrate formed by the protein's own C-terminus.

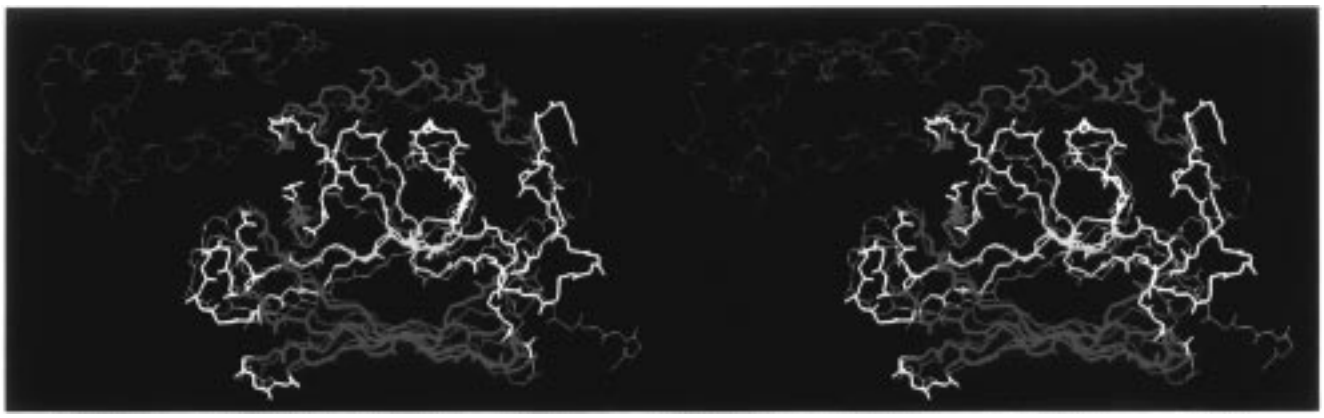

FIGURE 6: Superimposition of the backbone traces of DnaK 389−603, as determined from X-ray crystallography (*23*) (PDB accession code 1DKZ) (thin lines) and DnaK 386−553, as determined from NMR (thick lines). Color coding for the NMR structure is as in Figure 3. The location of the bound peptide NRLLLTG in the crystal structure is shown in red. The RMSD of superposition for the β-domains is 2.20 Å (backbone).

a peptide. This study thus shows conclusively that the relevant protein-binding site in Hsp70 chaperones is indeed located at the substrate-binding groove as identified by the work of Hendrickson and co-workers (*23*).

Substrate Binding Interactions. The interaction between DnaK and itself is remarkably similar to the interaction of DnaK with a peptide as described in the X-ray structure. Multiple interactions involving conserved residues are present at the substrate-binding site (Figures 6 and 8). The sequence of the C-terminus that binds to the binding site is ^{540}DHLLHSTR^{547} with the Hsp70 site "0" corresponding to the second leucine (L543). The side chain of this residue, but only this residue, is captured in a very deep hydrophobic pocket (Figure 8). The pocket is formed by residues I401, M404, L411, F426, A429, V436, I438, and I472 and V474. These residues are virtually conserved among different Hsp70 species (see Figure 1). The two residues M404 and A429 are located at the tip of the binding site and form a gate for the entrance of substrate. This gate is conserved among species by always having two hydrophobic residues paired, one large and one small, as already noted by others (*11*, *23*) (see Figure 1 and Figure 8). A leucyl residue was also found deeply in the same binding pocket in the X-ray structure (*23*). It is interesting to note that leucine is also found to be by far the most abundant amino acid in DnaK-binding sites as identified by screening (*11*, *58*). The side chains of the other residues in the extended binding region in the average NMR structure are fairly exposed. However, as considerable spread of the locations of these side chains is found in the different structures of the NMR ensemble, we cannot exclude that such residues do at least spend some time closer to the β-domain residues, likely in rapid dynamic equilibrium especially for the peripheral residues (see Figure 5). The length of the binding site is limited because it is along the short dimension of the molecule (28 Å). This confirms the optimal peptidic length of seven residues as was observed in binding studies (*6*−*11*). The interaction of the unwound chain is clearly not only driven by the interaction with a single hydrophobic side chain: the chain is placed in the groove with the same polarity as the peptide in the crystal

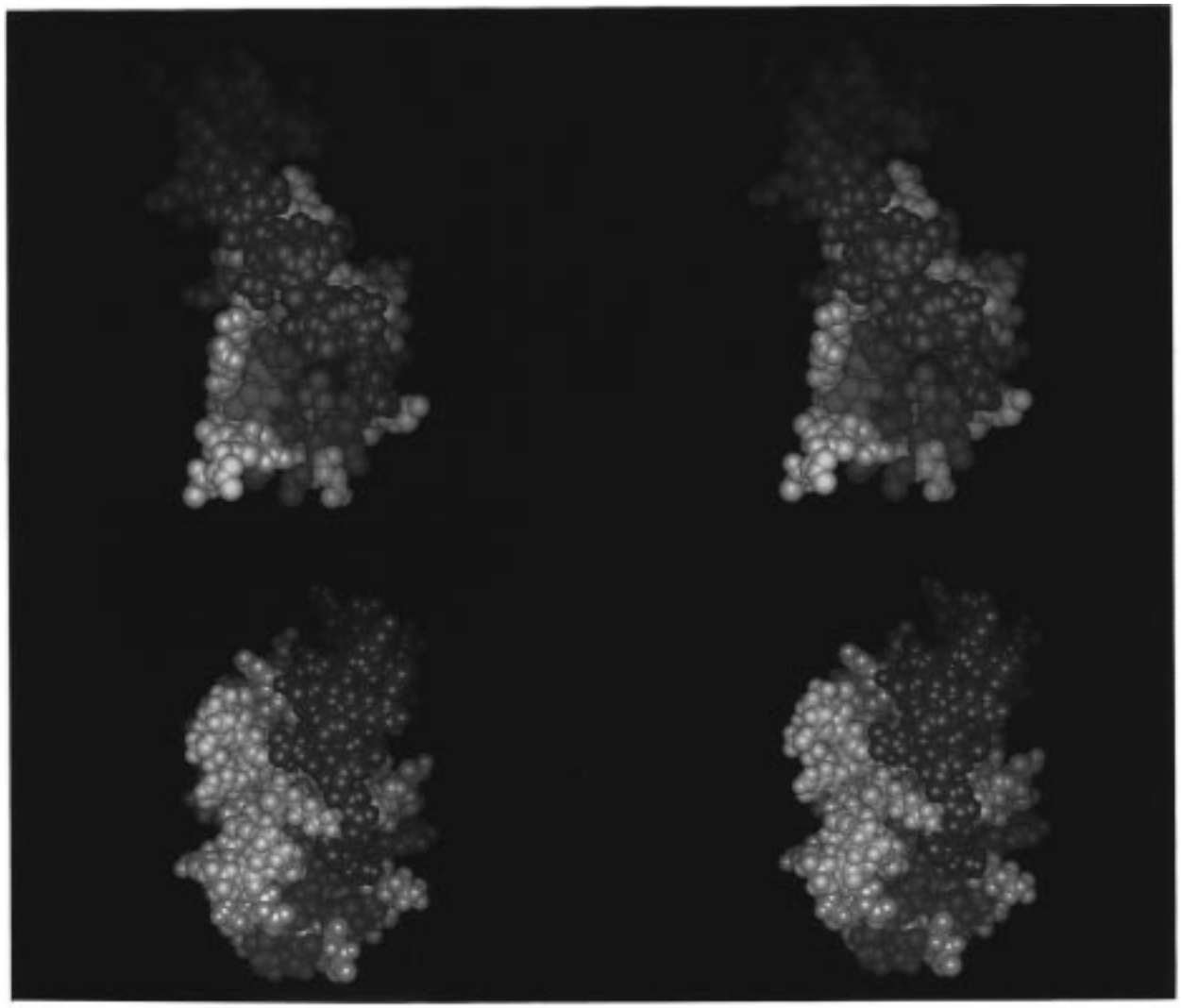

FIGURE 7: Front views of the X-ray (top) and NMR (bottom) structures of DnaK accentuating the differences in helix position (viewing from the right-hand side compared to Figure 3). The relative orientations were defined from best super position of the β-sheet domains. The apolar residues in each structure are green. The N-termini are yellow, the helix red, and the residues constituting the secondary hydrophobic binding site as discovered from paramagnetic peptide binding (residues L392, L397, A413, V394, T395, L484) are blue.

structure of DnaK, while it must be less entropically costly for the chain to enter the DnaK-substrate binding site from the "back" (in the orientation of Figure 4, see Figure 7) as the helix runs already on the back. At the current resolution, we cannot be certain which interactions are dictating the observed polarity of the binding. It may be possible that the electrostatic interaction of "substrate" residue Arg 547 with residue Asp 460 on the back of the β-domain generates this preference of orientation. Positively charged peptides appear to interact more strongly with DnaK than with other Hsp70s (*8*, *9*, *59*). We propose that electrostatic interaction of the positively charged peptides with side chain of residue Asp 460 is responsible for this phenomenon, as this location is occupied by Thr or Ser in other chaperones (see Figure 1).

DnaK−Protein Interactions. The current structure yields insight in the action of DnaK-SBD on folded proteins. From the crystal structure, it is known that the region of DnaK that interacts with the substrate binding site in solution is α-helical in its native state. Nevertheless, this region is unwound and placed in extended form in the substrate binding groove. Hsp70 chaperones have been predicted to be able to unwind entire protein regions and α-helices in particular (*11*). That is exactly what one now observes directly in the NMR structure of the DnaK fragment. Significant unfolding of the native state and thus stabilization of a more open state of substrate proteins by molecular chaperone action has also been deduced indirectly for the GroEL class (*60*, *61*). It has long been known that the heat shock proteins can rescue proteins from aggregation complexes (*62*, *63*). Significant unfolding action combined with release is likely to be necessary to accomplish such feats (*64*); the current study shows that DnaK is certainly capable of carrying out the unfolding.

It is most likely that the observed *self*-binding of DnaK in the NMR structure is a mere artifact of this specific protein construct. However, one should not totally discard the possibility that this process also occurs in vivo for the full Hsp70 protein. Residues Leu 542 and Leu 543, the latter of which is trapped in the binding cleft in the NMR structure of DnaK, are internal hydrophobic residues in the α-helical bundle in the crystal structure (Figure 9). Hydrophobic residues at these positions are conserved in the Hsp70 chaperones (Figure 1). It is, however, striking that these residues, for *E. coli* DnaK, are the only hydrophobic ones in the long helix for a stretch of 16 residues (see Figure 9

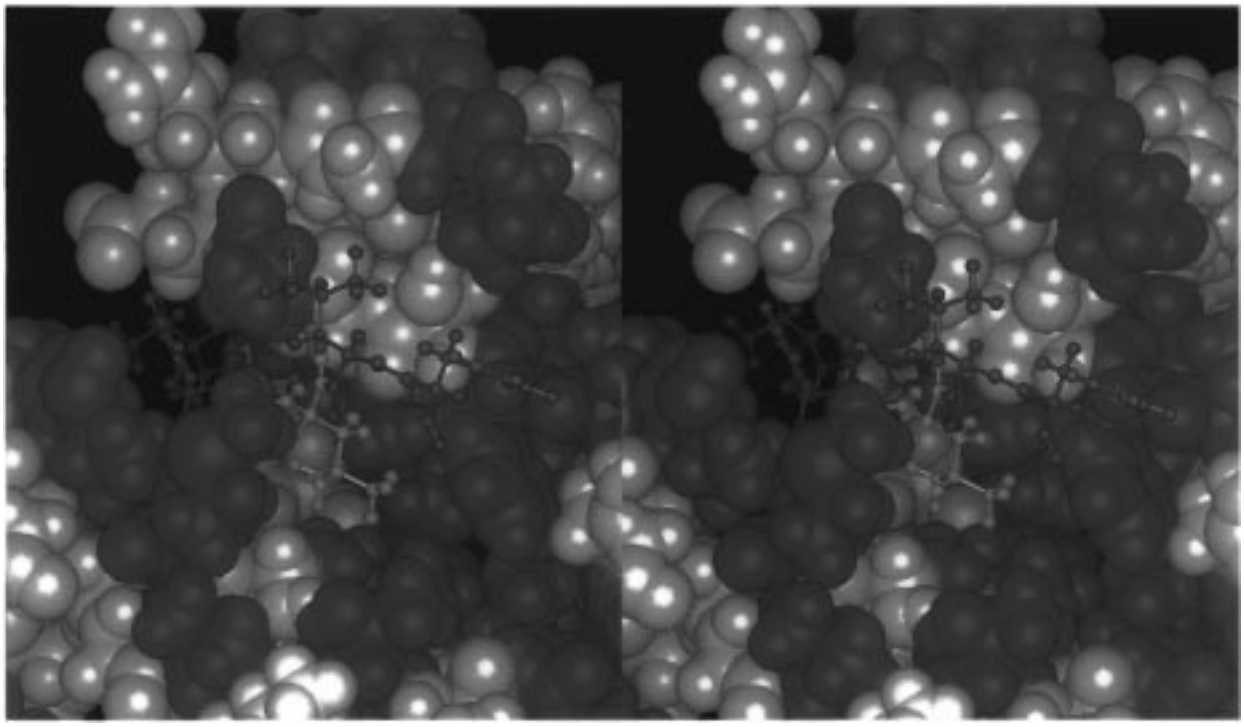

FIGURE 8: Details of the primary protein/peptide-binding site of DnaK 386−553 as determined from NMR. The simulated annealing structure with the lowest total energy is depicted. Space filling shells for apolar residues are shown in green, for polar residues in white. The C-terminal substrate of the NMR structure is shown in red, with residue Leu 543 located in the primary binding pocket, in yellow.

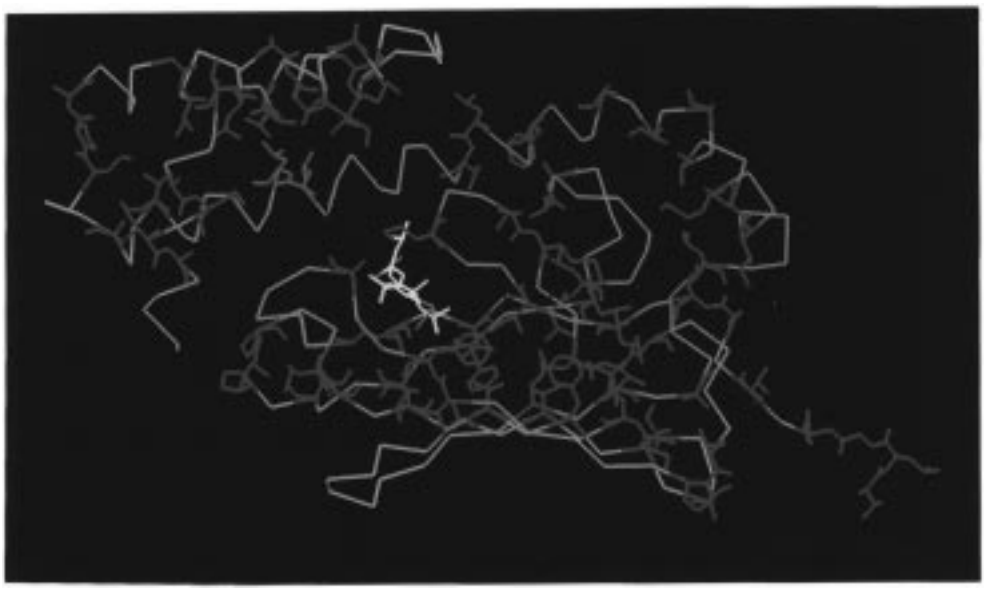

FIGURE 9: The hydrophobic residues (A, V, L, I, P, F) in the crystal structure of DnaK 389−603, as determined from X-ray crystallography are given in green, except for the residues Leu 542 and Leu 543 which are light-blue. The bound peptide is rendered red, with its apolar residues in yellow.

and Figure 1). It is thus not inconceivable that the helix is rather labile in this region and could, also in the full-length DnaK, be disrupted to give rise to an intramolecular (or intermolecular) complex. Such an association very effectively blocks the binding site (see below). Ability to reach an "off-state" for this potentially harmful protein-unfolding molecule could be very important for the survival of the cell. Against such a hypothesis argues the fact that there are complementary charge−charge interactions between this part of the helix and the loops of the β-domain in the crystal structure which may stabilize the helical conformation and thus interfere with self-binding (see Figure 5B of ref *23*). Furthermore, lack of hydrophobicity in this area of the helix is not strictly conserved between species (Figure 1), where, especially for the eukaryotic Hsp70s, a classical amphipathic amino acid composition is seen. Nevertheless, the definitive absence of an amphipathic pattern in the DnaK helix remains intriguing.

Delineation of a Secondary Binding Site. We carried out NMR studies to detect peptide binding to the fragment DnaK 386-561. Peptides used were the so-called peptides A $(KRQIYTDLEMNRLGK)^7$, K $(KLIGVLSSLFRPK)^7$, and a peptide G (VKKRCSMWIIPTDDEA) as discovered by one of us (G.C.F.). These peptides bind tightly to full-length

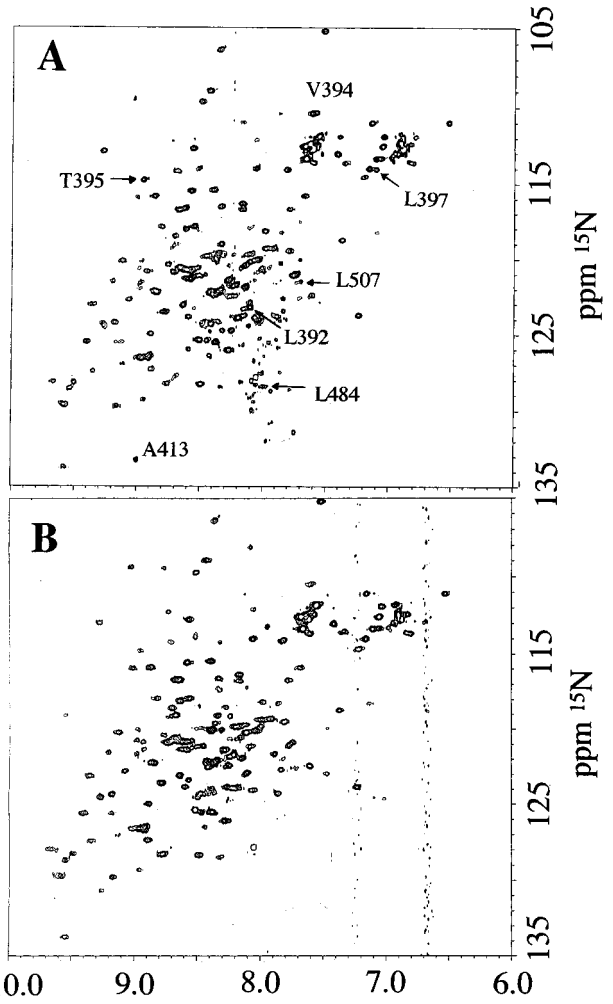

FIGURE 10: Amide nitrogen-proton shift correlation experiments (^{15}N HSQC) of 0.2 mM DnaK 386−553 in 50 mM phosphate buffer, pH 7.0, 25 °C, 500 MHz (^{1}H). Panel A, the spectrum in the absence of peptides; panel B, the spectrum in the presence of the peptide KLIGVLCSLFRPK, labeled with the paramagnetic nitroxide label TEMPO at Cys 7. The peptide is present in slight excess over the protein. Protein resonances that disappeared or significantly attenuated upon addition of this agent are identified in panel A.

DnaK. The ^{15}N-^{1}H amide shift correlation map (^{15}N HSQC), as well as in some cases a three-dimensional ^{13}C-resolved NOE spectrum of double-labeled DnaK 386−561, was monitored while titrating in several of these peptides. Protein concentrations of 1 mM and peptide concentrations up to 10 mM were used. However, no significant shifts (fast exchange) or disappearances/appearances (slow exchange) of cross-peaks in the NMR spectra of DnaK-SBD were detected. This lead to the conclusion, now obvious, that the construct DnaK 386−561 is not binding peptides. Fluorescence data, however, did suggest that this very same construct does bind to the same peptides that do bind to full-size DnaK, albeit with less potency (G. Walker, personal communication); in addition, the homologous fragment from Hsc was reported to have a peptide-binding affinity (8 μM) indistinguishable from that of the native Hsc70 (5−8 μM) for the S-peptide of Rnase-A (*24*). To further investigate binding using NMR spectroscopy, paramagnetically labeled peptides were titrated into a solution of ^{15}N-labeled DnaK-SBD while the ^{15}N-^{1}H amide shift correlation map was monitored by NMR (Figure 10). Three NH correlations (L392, L397, and A413) disappeared completely from the NMR map upon addition of slight excess of TEMPO peptides, while four more resonances (V394, T395, L484, and L507) were significantly weakened (broadened). The resonances returned to their original intensities when the spin label was reduced with ascorbic acid in the NMR tube containing the mixture (result not shown). This established that the disappearance and weakening of the resonances was due to paramagnetic broadening. These observations suggest that the modified peptides do indeed bind to DnaK-SBD. However, it was found that the same resonances disappeared for three different peptides used. It was concluded that it is the hydrophobic spin label itself that interacts with DnaK-SBD, with the attached peptides merely serving to solubilize the label. Figure 7 shows the location of the residues that exhibited paramagnetically broadened resonances. The residues are conserved between the species, except for Ala 413, as shown in Figure 1. It is immediately apparent, especially in the crystal structure, that these residues that bind the hydrophobic spin label form a contiguous hydrophobic patch remote from the primary substrate-binding site (Figure 7). The patch is partially covered up in the NMR structure by the N-terminus of the protein. The position of the N-terminus is determined by a single NOE; therefore, it is likely that it can swing away part of the time to allow access for the spin label. It is possible that binding to this hydrophobic patch accounted for the transferred NOEs in peptide K in the presence of DnaK (*65*); the primary binding site of DnaK could not have contributed to the transferred NOE because (*66*) its dissociation rate is too slow by at least 2 orders of magnitude (*67, 68*).

Possible Function of the Secondary Binding Site for the Coupling Mechanism. Full-size DnaK binds tightly to hydrophobic patches on partially unfolded proteins in the ADP-bound form. Upon ATP binding, the protein changes conformation and the kinetics of binding and release of hydrophobic patches on partially unfolded proteins is greatly enhanced leading to substrate release or exchange (*14, 69*). As nucleotide binding takes place in the ATPase domain while substrate binding takes place in the substrate-binding domain, this modulation of kinetics must be due to long-range allosteric interactions. Recent studies have shown that nucleotide-dependent interdomain communication requires, besides the ATPase domain, only the first 15 kDa of the substrate-binding domain, i.e., the SBD fragment that is being studied here (*11, 66*). As the ATPase domain could be crystallized independently (*21*) while the substrate binding domain has a defined solution conformation, we must conclude that these domains are more or less independent structural entities in the complete molecule. The transmittal of information between the ATPase domain and substrate-binding domain must thus take place through a relatively small interdomain interface. Figure 7 shows that the C-terminal helix of the NMR substrate-binding domain is considerably displaced from the position of this helix in the crystal structure of the full substrate-binding domain. Nevertheless, the conformation of the β-domain is identical in both structures. This demonstrates that the location of the helical bundle domain with respect to the β-domain is much more variable than suggested by Hendrickson and co-workers (*23*). Our data indicates that the helical domain can pivot on the β-domain with a pivot point located at the base of the helix in the area around residue 508. The ^{15}N NOE data

suggest flexibility for this area as well (see Figure 5). The number of NOE distance constraints observed between the helix proper and the β-domain is very limited (10), and it is not unlikely that the here-reported location for the helix is only the dominant one of many possibilities. The dynamics of such putative motion is not very fast as we do not see exchange broadening of the resonances of the helix (which would require time scales of 10^{-5} to 1 s) nor observe excessive local motion for the N−H vectors of residues in this helix as measured from ^{15}N NOE data (which would require time scales of 10^{-9} s or shorter).

Much larger displacements of the helix must be expected for functioning Hsp70 proteins from the point of view that they interact with complete proteins and not only with small hydrophobic peptides. DnaK must be able to expose its binding site considerably more than merely offering an internal channel. The huge activation enthalpies measured for peptide association and dissociation (26 and 34.6 kcal/mol, respectively (*67*)) also suggest that major conformational changes are required for substrate exchange. The conformation as found in the crystal structure might thus represent DnaK in the slow-exchange (ADP) conformation, while location of the α-helix in the NMR structure could represent one of the more loose (ATP) conformations that allow rapid substrate exchange, or, possibly, a totally inactive conformation if the self-association is relevant (see above). Further elucidation of this point should await the structure elucidation of DnaK complexed to another protein.

It is interesting to observe that the N-terminus of the helix αA in the crystal structure partially interacts with a hydrophobic patch on the β-domain (Figure 7); this patch is partially overlapping with the second binding site as detected by the paramagnetic peptide binding discussed above (Figure 10). In the NMR structure, this patch is mostly overlapped with the N-terminal 10 residues (Figure 7). As this interaction is disclosed by only a single NOE (V386-A449) it is likely to be only a subpopulation of possible locations for the N-terminus, at least for this protein construct. The residues in the N-terminus are strongly conserved hydrophobic and constitute the transition region between the ATPase and substrate-binding domain (Figure 1). Why would such conservation pertain if this was only a floppy interdomain loop? To rationalize these findings, we propose the following model for the transduction of signal from the ATPase domain to the substrate-binding site, which is an extension on the current models proposed recently (*23*, *58*). In the ADP conformation, the base of the helix interacts with the hydrophobic patch on the β-domain. In this conformation, the helix overlays the substrate-binding groove retaining bound substrate/protein. Upon conformational change in the ATPase domain, the leucine-rich transition region competes for the hydrophobic patch on the β-domain and displaces the base of the helix, leading to an overall displacement or a dynamical structure for this helix that can easily release bound substrate and accept free substrate.

CONCLUSIONS

The self-binding of the DnaK substrate-binding domain offers a preview of the interaction of this chaperone with other proteins. The bound protein region is coerced into an extended conformation, while its native structure is α-helical. The bound protein region is tightly held at a single amino acid position (a leucyl residue) that is buried in a deep pocket lined with conserved hydrophobic residues. A second hydrophobic-binding site has been identified. It is located in a region close to the N-terminus of the domain. It is hypothesized that this region is competed for by the N-terminus of the α-helical domain of the substrate-binding domain and the transition region linking the ATPase and substrate-binding domain. This competition may constitute the allosteric mechanism that links substrate-binding affinity with nucleotide binding in the Hsp70 chaperones.

ACKNOWLEDGMENT

Mr. E. Bertelsen (University of Oregon) is acknowledged for participation in the protein preparation. We thank Mr. R. T. Gampe (Glaxo-Wellcome, Research Triangle Park, NC) for making the NMR data interpretation software RGO available. We are much indebted to Dr. G. Walker (MIT) for sending us variants of peptide K.

SUPPORTING INFORMATION AVAILABLE

The coordinates of the average structure and of the ensemble of 25 structures are available in protein data bank format. Access information is given on any current masthead page.

REFERENCES

1. Yochem, J., Uchida, H., Sunshine, M., Saito, H., Georgopoulos, C. P., and Feiss, M. (1978) *Mol. Gen. Genet. 164*, 9−14.
2. Hendrick, J. P., and Hartl, F. U. (1993) *Annu. Rev. Biochem. 62*, 349−384.
3. Craig, E. A., Gambill, B. D., and Nelson, R. J. (1993) *Microbiol. Rev. 57*, 402−414.
4. Georgepoulos, C. (1994) in *The Biology of Heat Shock Proteins and Molecular Chaperones*, (Morimoto, R. I., Tissieres, A., and Georgepoulos, C., Eds.) pp 209−249, Cold Spring Harbor Laboratory Press, Plainview, NY.
5. Martin, J., and Hartl, F. U. (1997) *Curr. Opin. Struct. Biol. 7*, 41−52.
6. Flynn, G. C., Chappell, T. G., and Rothman, J. E. (1989) *Science 245*, 385−390.
7. Flynn, G. C., Pohl, J., Flocco, M. T., and Rothman, J. E. (1991) *Nature 353*, 726−730.
8. Gragerov, A., Zeng, L., Zhao, X., Burkholder, W., and Gottesman, M. E. (1994) *J. Mol. Biol. 235*, 848−854.
9. Fourie, A. M., Sambrook, J. F., and Gething, M. J. (1994) *J. Biol. Chem. 269*, 30470−30478.
10. Rüdiger, S., Germeroth, L., Schneider-Mergener, J., and Bukau, B. (1997) *EMBO J. 16*, 1501−1507.
11. Rüdiger, S., Buchberger, A., and Bukau, B. (1997) *Nat. Struct. Biol. 4*, 342−349.
12. Zylicz, M., DeBowitz, J., McMacken, R., and Georgepoulis, C. (1983) *Proc. Natl. Acad. Sci. U.S.A. 80*, 6431−6435.
13. Palleros, D. R., Reid, K. L., Shi, L., Welch, W. J., and Fink, A. L. (1993) *Nature 365*, 664−666.
14. McCarty, J. S., Buchberger, A, Reinstein, J., and Bukau, B. (1995) *J. Mol. Biol. 249*, 126−137.
15. Langer, T., Lu, C., Echols, H., Flanagan, J., Hayer, M. K., and Hartl, F. U. (1992) *Nature 356*, 683−689.
16. Liberek, K., Marszalek, J., Ang, D., Georgepoulos, C., and Zylicz, M. (1991) *Proc. Natl. Acd. Sci. U.S.A. 88*, 2874−2878.
17. Harrison, C. J., Hayer-Hartl, M., Di Liberto, M., Hartl, F. U., and Kuriyan, J. (1997) *Science 276*, 431−435.
18. Szabo, A., Langer, T., Schröder, H., Flanagan, J., Buchau, B and Hartl, F. U. (1994) *Proc. Natl. Acad. Sci. U.S.A. 91*, 10345−10349.
19. Hartl, F. U., and Martin, J. (1995) *Curr. Op. Struct. Biol. 5*, 92−105.

20. Pierpaoli, E. V., Sandmeier, E., Baici, A., Schönfeld, H.-J., Gisler, S., and Christen, P. (1997) *J. Mol. Biol. 269*, 757−768.
21. Flaherty, K. M., DeLuca-Flaherty, C., and McKay, D. B. (1990) *Nature 346*, 623−628.
22. Chappell, T. G., Konforti, B. B., Schmid, S. L., and Rothman, J. E. (1987) *J. Biol. Chem. 262*, 746−751.
23. Zhu, X., Zhao, X., Burkholder, W. F., Gragerov, A., Ogata, C. M., Gottesman, M. E., and Hendrickson, W. A. (1996) *Science 272*, 1606−1614.
24. Wang, T.-F., Chang, J.-H., and Wang C. (1993) *J. Biol. Chem. 268*, 26049−26051.
25. Cyr, D. M., Langer, T., and Douglas, M. G. (1994) *Trends Biochem. Sci. 19*, 176−181.
26. Wawrzynow, A., Banecki, B., Wall, D., Liberek, K., Georgopoulos, C., and Zylicz, M. (1995) *J. Biol. Chem. 270*, 19307−19311.
27. Wawrzynow, A., and Zylicz, M. (1995) *J. Biol. Chem. 270*, 19300−19306.
28. Morshauser, R. C., Wang, H., Flynn, G. C., and Zuiderweg, E. R. P. (1995) *Biochemistry 34*, 6261−6266.
29. Wang, H. (1995) Ph.D. Thesis. The University of Michigan.
30. Rippmann, F., Taylor, W., Rothbard, J., and Green, N. M. (1991) *EMBO J. 10*, 1053−1059.
31. Gragerov, A., Nudler, E., Komissarova, N., Gaitanaris, G. A., Gottesman, M. E., and Nikiforov, V. (1992) *Proc. Natl. Acad. Sci. U.S.A. 89*, 10341−10344.
32. Neidhardt, F. C., Bloch, P. L., and Smith, D. F. (1974) *J. Bacteriol. 119*, 736−747.
33. Grzesiek S., and Bax, A. (1992) *J. Magn. Reson. 96*, 432−440.
34. Olejniczak, E. T., Xu, R. X., Petros, A. M., and Fesik, S. W. (1992) *J. Magn. Reson. 100*, 444−450.
35. Clubb, R. T., Thanabal, V., and Wagner, G. (1992) *J. Biomol. NMR 2*, 389−394.
36. Boucher, W., Laue, E. D., Campbell-Burk, S., and Domaille, P. J. (1992) *J. Biomol. NMR 2*, 631−637.
37. Zuiderweg, E. R. P. (1990) *J. Magn. Reson. 89*, 533−542.
38. Brown, L. R., and Sanctuary, B. C. (1991) *J. Magn. Reson. 91*, 413−421.
39. Majumdar, A., Wang, H., Morshauser, R. C., and Zuiderweg, E. R. P. *(1993) J. Biomol. NMR 3*, 387−397.
40. Wang, H., and Zuiderweg, E. R. P. (1995) *J. Biomol. NMR 5*, 207−211.
41. Bax, A., Clore, G. M., and Gronenborn, A. M. (1990) *J. Magn. Reson. 88*, 425−431.
42. Fesik, S. W., Eaton, H. L., Olejniczak, E. T., Zuiderweg, E. R. P., McIntosh, L. P., and Dahlquist, F. W. (1990) *J. Am. Chem. Soc. 112*, 886−888.
43. Clore, G. M., and Gronenborn, A. M. (1994) *Methods Enzymol. 239*, 349−363.
44. Fischer, M. W. F., Zeng, L., and Zuiderweg, E. R. P. (1996) *J. Am. Chem. Soc. 49*, 12457−12458.
45. Fesik, S. W., and Zuiderweg, E. R. P. (1988) *J. Magn. Reson. 78*, 588−593.
46. Piotto, M., Saudek, V., and Sklenar, V. (1992) *J. Biomol. NMR 2*, 661−665.
47. Clore, G. M., Kay, L. E., Bax, A., and Gronenborn, A. M. (1991) *Biochemistry 30*, 12−18.
48. Zuiderweg, E. R. P., Petros, A. M., Fesik, S. W., and Olejniczak, E. T. (1991) *J. Am. Chem. Soc. 113*, 370−372.
49. Kuboniwa, H., Grzesiek, S., Delaglio, F., and Bax, A. (1994) *J. Biomol. NMR 4*, 871−878.
50. Kay, L. E., Torchia, D. A., and Bax, A. (1989) *Biochemistry 28*, 8972−8979.
51. Dayie K. T., and Wagner, G. (1994) *J. Magn. Reson. A111*, 121−126.
52. Lipari, G., and Szabo, A. (1982) *J. Am. Chem. Soc. 104*, 4546−4559.
53. Zheng, Z., Czaplicki, J. and Jardetzky, O. (1995) *Biochemistry 34*, 5212−5223.
54. Wüthrich, K. (1986) *NMR of Proteins and Nucleic Acids*, John Wiley, New York.
55. Nilges, M., Gronenborn, A. M., Brunger, A. T., and Clore, G. M. (1988) *Protein Eng. 2*, 27−38.
56. Zeng, L., Fischer, M. W. F., and Zuiderweg, E. R. P. (1996) *J. Biomol. NMR 7*, 157−162.
57. Fischer, M. W. F., Zeng, L., Pang, Y., Hu, W., Majumdar, A., and Zuiderweg, E. R. P. (1997) *J. Am. Chem. Soc. 119*, 12629−12642.
58. Rüdiger, S., Germeroth, L., Schneider-Mergener, J., and Buchau, B. (1997) *EMBO J. 16*, 1501−1507.
59. De-Crouy-Chanel, A., Kohiyama, M., and Richarme, G. (1996) *J. Biol. Chem. 271*, 15486−15490.
60. Martin, J., Langer, T., Boteva, R., Schramel, A., Horwich, A. L., and Hartl, F. U. (1991) *Nature 352*, 36−42.
61. Zahn, R., Spitzfaden, C., Ottiger, M., Wüthrich, K., and Pluckthun, A. (1994) *Nature 368*, 261−264.
62. Lindquist, S. (1987) *Annu. Rev Biochem 55*, 1151−1191.
63. Ziemienowicz, A., Skowyra, D., Zeilstra-Ryalls, J., Fayet, O., Georgopoulos, C., and Zylicz, M. (1993) *J. Biol. Chem. 268*, 25425−25431.
64. Sfatos, C. D., Gutin, A. M., Abkevich, V. I., and Shakhnovitch, E. I. (1996) *Biochemistry 25*, 334−339.
65. Landry, S. J., Jordan, R., and Gierash, L. M. (1992) *Nature 355*, 455−457.
66. Clore, G. M., and Gronenborn, A. M. (1983) *J. Magn. Reson. 53*, 423−442.
67. Farr, C. D., Galiano, F. J., and Witt, S. N. (1995) *Biochemistry 34*, 15574−15582.
68. Palleros, D. R., Reid, K. L., Shi, L., Welch, W. J., and Fink, A. L. (1993) *Nature 365*, 664−666.
69. Buchberger, A., Theyssen, H., Schröder, H., McCarty, J. S., Virgallita, G., Milkereit, P., Reinstein, J., and Bukau, B. (1995) *J. Biol. Chem. 270*, 16903−16910.

BI9800855